Journal of Cultural Heritage 49 (2021) 19–27

Contents lists available at ScienceDirect

Journal of Cultural Heritage

journal homepage: www.elsevier.com/locate/culher

Original article

A new application of Fiber optics reflection spectroscopy (FORS): Identification of "bronze disease" induced corrosion products on ancient bronzes

Wei Liu[a,b], Mo Li[b], Na Wu[b], Siran Liu[c], Jianli Chen[a,*]

[a] Peking University, School of Archaeology and Museology, No. 5 Yiheyuan Road, Haidian District, 100871 Beijing, China
[b] National Museum of China, the Conservation Center, No. 248 Shiliuzhuang West Steet, Fengtai District, 100079 Beijing, China
[c] University of Science and Technology Beijing, Institute for Cultural Heritage and History of Science & Technology, No. 30 Xueyuan Road, Haidian District, 100083 Beijing, China

ARTICLE INFO

Article history:
Received 11 January 2021
Revised 18 March 2021
Accepted 18 March 2021
Available online 15 April 2021

Keywords:
FORS
Bronze disease
Corrosion products
Copper trihydroxychloride
Chalconatronite

ABSTRACT

Fiber Optics Reflectance Spectroscopy (FORS) has been widely used in the field of cultural heritage for material identification. Nevertheless, it had been rarely applied in the study of bronze corrosion products. This paper aims at exploring the potential of FORS on corrosion products analysis, proposing it as an innovative non-destructive technique for the condition assessment of bronze artefacts in museum collections. A gilded bronze statue "Vajrasattva Bodhisattva" dated to the Ming dynasty (A. D. 1368-1644) from National Museum of China was investigated. The in-situ FORS analysis was conducted on 36 points, revealing copper trihydroxychloride (atacamite/clinoatacamite) and chalconatronite as two major types of corrosion products. This result was double-confirmed by Raman and XRD analyses of 10 samples taken from these points. It proves that FORS is a very promising technique for non-destructive in-situ detection of chloride-bearing bronze corrosions. It may revolutionize the way of screening artefacts with bronze disease, helping conservators get the distribution "map" of different bronze corrosion quickly and comprehensively, and making appropriate treatment proposals accordingly.

Research aims

This study aims at developing Fiber optics reflection spectroscopy (FORS) in visible, near-infrared (VNIR) and short-wave infrared (SWIR) spectral regions (350-2400 nm), as a non-destructive in-situ method for identifying the corrosion products on bronze artefacts. This new application of FORS allows conservators to quickly assess the preservation condition of artefacts and make a proper treatment proposal.

1. Introduction

The ancient bronzes are often found being covered with layers of corrosion. Various types of the corrosion products with different chemical composition, stability and physical characteristics, could be formed depending on the burial or storage environment [1–8]. Generally, the typical corrosion products appearing on bronzes in museum environment include copper oxides (cuprite Cu_2O and tenorite CuO), basic copper carbonate (malachite $CuCO_3{\cdot}Cu(OH)_2$, azurite $2CuCO_3{\cdot}Cu(OH)_2$, chalconatronite $Na_2Cu(CO_3)_2{\cdot}3H_2O$,) copper chlorides and basic copper chlorides (nantokite CuCl, atacamite $Cu_2(OH)_3Cl$, clinoatacamite, paratacamite, botallackite), copper phosphates (liberthenite $Cu_2(PO_4)(OH)$), copper nitrates (gerhardtite, $Cu_2(NO_3)(OH)_3$) and the organic salts of copper (copper formates and acetates) [5]. Among those corrosion products, the copper chlorides and basic copper chlorides are mostly concerned by conservators, because their formation are closely related to "bronze disease".

The bronze disease is well-known as the major threat of bronze preservation due to severe damage on metallic body and its high developing rate [1,3,5,6,9–18]. The corrosion products formed in this process mainly involve cuprous chloride (CuCl, nantokite) and copper trihydroxychloride ($2Cu_2(OH)_3Cl$, atacamite, clinoatacamite, paratacamite and botallackite) (Table 1). Thus, the presence of these chloride-containing corrosion products was usually taken as the major indicator of bronze disease.

The accurate identification of these bronze corrosion products is important for conservators to make treatment proposals. The common methods for identifying bronze disease-related cor-

* Corresponding author.
E-mail address: jianli_chen@pku.edu.cn (J. Chen).

https://doi.org/10.1016/j.culher.2021.03.007
1296-2074/

Table 1
Characteristics of bronze disease induced corrosion products [5,13].

Corrosion products' name	Formula	Crystal system	color
Nantokite	CuCl	Cubic	Pale green
Atacamite	$Cu_2(OH)_3Cl$	Orthorhombic	Dark green
Clinoatacamite	$Cu_2(OH)_3Cl$	Monoclinic	Pale green
Paratacamite	$(Cu,Zn)_2(OH)_3Cl$	Rhombohedral	Pale green
Botallackite	$Cu_2(OH)_3Cl$	Monoclinic	Pale green

rosion products include various laboratory-based analytical techniques, such as scanning electron microscope coupled with energy-dispersive X-ray detection (SEM-EDX), X-ray Florescence (XRF), Raman spectroscopy, Infrared spectroscopy and X-ray diffraction (XRD). In particular, XRD is a well-developed method for phase identification of the mixed bronze corrosion products qualitatively and quantitatively, and often used to verify the results acquired by other techniques [5,19]. Raman spectroscopy has been widely applied in recent decades and proved to be particularly suitable for the identification of minor Cl-bearing mineral components in corrosion products [20–23]. However, the corrosion samples could only be selected based on their color, morphology and texture with little instrumental aid. The representativeness of these samples is usually questionable and could be influenced by the complex nature of corrosion products and the experience of conservators. Due to these problems, it is difficult to acquire an accurate picture of objects corrosion state only based on aforementioned analytical techniques, which may then lead to an uncomprehensive assessment of their preservation conditions and inappropriate conservation proposal.

Fiber optics reflection spectroscopy (FORS) is a well-established non-invasive method used in the field of cultural heritage. It has been widely used for the identification of pigments [24–36], dyes [37–40], binders [41,42], iron-gall ink [43], textile [44], and modern restoration materials [45]. It was also used to investigate the degradation of the glass [46] and plastic materials used in 20th century artworks [47]. Furthermore, the imaging version of reflectance spectroscopy (hyperspectral imaging) has been used for restoring the covered pattern and distinguishing the pigments on the surface of the bronze chariot [48], and investigating the distribution of different corrosion phases on iron artifacts [49].

A number of organizations including Institute for Applied Physics "Nello Carrara" of the Italian National Research Council (IFAC-CNR) and the United States Geological Survey (USGS) have established the FORS databases for natural pigments or minerals. Some research groups have also built their own in-house spectral databases [34,50]. Among these databased pigment spectra, we noticed that some copper-bearing minerals such as malachite, azurite, are also the major corrosion products of bronze. Moreover, the bronze disease induced corrosion products such as atacamite, paratacamite and botallackite have also been reported to be used as pigments on paintings, manuscripts and polychrome sculptures, although it is doubted by scholars if the minerals are original pigments themselves or alteration products from the transformation of original pigments [5,51]. It was, however, found that atacamite and malachite present a very similar spectral features in VIS-NIR spectral region (350-1000 nm) and not easily distinguished in this wavelength range. The hope of separating these two minerals by FORS lays on the range of 1000-2500 nm. The atacamite spectrum in the range of 1000-2500 nm is not easily accessible to the best of the authors' knowledge. Li [52] mentioned that malachite and atacamite could be differentiated in the wavelength range of 400-2500 nm, but did not introduce the spectral difference in detail. Catelli [53] studied the spectral features of atacamite as corrosion products firstly in the NIR-MIR region, but did not compare the spectrum of atacamite with that of other corrosion products including malachite. Given this background, we attempted to build our own standard spectra of malachite, atacamite as well as other corrosion products commonly found on bronzes, and establish FORS as a technique to differentiate various types of bronze corrosion products. This method was then applied to a gilded bronze statue "Vajrasattva Bodhisattva", mapping the spatial distribution of different corrosion products with special attention to copper trihydroxychloride.

Fig. 1. The gilded bronze statue "Vajrasattva Bodhisattva" from the collections of National Museum of China. Left: Frontal view, Right: Side view.

2. Description of the object and the conservative problem

The gilded bronze statue "Vajrasattva Bodhisattva" is dated to Ming dynasty (A. D. 1368-1644) and collected in National Museum of China since 2001 (Fig. 1). The statue was gilded and details of the crown, belt, arms and legs were highlighted with inlaid turquoise blue semi-precious stones, though some of these insets have fallen off. A small amount of blue pigments could be observed on the back side of the head.

The bronze statue was transferred to the Conservation Center in National Museum of China for condition assessment and treatment after a preliminary investigation. It is 30 cm in height and the widest part is 19 cm. In general, the object is intact but disfigured by some patches of light green corrosion products. The frontal and left-hand side was deteriorated more severely than the back. The green corrosion products could be observed on the statue's crown, head, face, hands, legs and the lotus throne. In some areas, the original gilded layer was destroyed by the chalky patches of corrosion products (Fig. 2). Most of the corrosion products present a light green powdery look, voluminous in texture which easily fall off, which was commonly taken as a sign of bronze disease. In order to distinguish copper chloride or copper trihydroxychloride, and get a distribution "map" of different corrosion products, in-situ FORS measurement combined with laboratory methods were performed.

Fig. 2. Light green powdery corrosion products observed on different areas on the surface of the gilded bronze statue. a. The head of the bronze statue, part of gilding surface was destroyed; b. The beads on lotus throne covered with light green corrosion products; c. The hands of the bronze statue, patches of light green products were found on the back and fingers of the hands as well as the wrist; d. The left leg of the statue, the engravings were covered by corrosion products.

3. Experimental

3.1. Samples

Thirty six spots of green powdery corrosion on the bronze statue were measured by FORS non-invasively. Among them, ten positions were also invasively sampled in order to verify the results obtained by FORS. Eight samples are about 0.01 grams in weight and the other two are about 0.1 grams, which are selected for XRD analysis. Samples were removed by a scalpel from the exterior and interior surfaces of the crown, forehead, finger, back of hand, leg and lotus throne. Sampling principle is mainly based on the appearance, such as color and texture.

Some pigments on historical paintings such as malachite and azurite, has been identified by FORS successfully. Pigments made by Kremer Pigment GmbH & Co (Aichstetten, Germany) were often used as reference samples in FORS analysis. Since the chemical composition of natural pigments and chemical reagents is identical with the corresponding corrosion products, three kinds of pigments including malachite (44400), azurite (10200) and atacamite (103901) from Kremer, and six kinds of chemical or analytical pure reagents including cuprous oxide, cupric oxide, cuprous chloride, basic copper sulphate, copper sulphate pentahydrate and copper hydroxide phosphate were selected as reference samples for corrosion identification in this study (Table 2). The chemical reagents were bought from Sinopharm Chemical Reagent Co., Ltd, Shanghai Macklin Biochemical Co., Ltd and Chengdu XiYa Chemical Technology Co., Ltd. The selected chemicals represent the most commonly found corrosion products on bronzes as well as those hardly distinguishable from appearance.

3.2. Methods

Fiber optic reflection spectroscopy measurements were carried out in situ on the bronze object. The analysis was performed with an Avantes AvaSpec-DUAL/ NIR DUAL spectrometer equipped with a 10W Tungsten halogen light source (AvaLight-HAL-S-Mini) and a VIS-NIR fiber (FCR-19UVIR200-2-ME). The optical fibers bundle is 2 meters in length, consisting of 19 single fibers. The single fiber is made of pure fused silica core, which is cladded with a fluorine doped fused silica and polyimide buffers. The core diameter of a single fiber is 200 μm. The probe end is jacketed with chrome-plated brass. The optical fibers bundle was applied to convey the radiation from the light source to the sample surface, and send the signal back to the spectrometers. A reflection stage was used to hold the fiber probe for measurements. The diffuse light is collected at the same angle of the incident light. The spectral resolution for VNIR (350-1100 nm) and SWIR (1060-2400 nm) is 4.8 nm and 16 nm respectively and the spectrum sampling interval is 0.6 nm and 5 nm respectively. The equipment was calibrated with a WS-2 white reference made out of PTEE, a diffuse based material provided by Avantes before each measurement. The material reflects light from 350 -1800 nm at circa 98% and from 250-2500 nm at more than 92%. The working distance is approximately 2 mm. The light spot size is about 5 mm in diameter. The software used to collect the spectra data is AvaSoft 8.0. Three spectra were acquired on each sample for statistical purposes.

Micro-Raman spectrometer Renishaw inVia (UK) with an air cooled DPSS laser operating at 50 mW and 532 nm was used for Raman analysis. A Leica microscope with magnification x50 LWD was used to allow the confocal measurements of the samples. The backscattered light was dispersed using 1800 l/mm grating. The

Table 2
Details of natural pigments and chemical reagents used as reference samples.

	Sample name	Formula	Purity	Item No.	CAS No.	Company
1	malachite	$CuCO_3$•$Cu(OH)_2$		44400		Kremer
2	azurite	$2CuCO_3$•$Cu(OH)_2$		10200		Kremer
3	atacamite	$Cu_2(OH)_3Cl$		103901		Kremer
4	cuprous oxide	Cu_2O	99%	20016796	1317-39-1	Sinopharm
5	cupric oxide	CuO	AR≥99.0%	10008018	1317-38-0	Sinopharm
6	cuprous chloride	CuCl	AR≥97.0%	10007718	7758-89-6	Sinopharm
7	basic copper sulphate	$CuSO_4$•$3Cu(OH)_2$	98%	C860758	1344-73-6	Macklin
8	copper sulphate pentahydrate	$CuSO_4$•$5H_2O$	AR,99%	C805353	7758-99-8	Macklin
9	copper hydroxide phosphate	$Cu_2(PO_4)(OH)$	≥97.0%	A35160	12158-74-6	XiYa

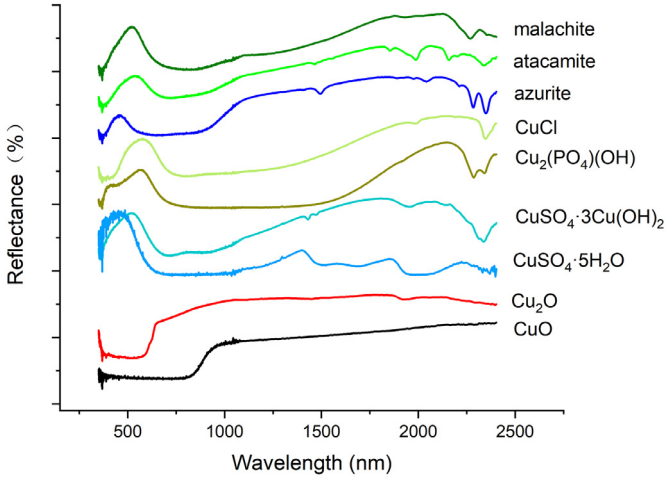

Fig 3. Reflectance spectra of nine reference samples

spectral resolution is 1-2 cm^{-1}. The laser power varied from 1-5%, The exposure time is 10 s. The accumulations are 2-4 times. The spectra were recorded in the range of 100 to 3800 cm^{-1}. The Renishaw WiRE 4.1 software was used for data acquisition and analysis.

X-ray diffraction (XRD) was used to determine the chemical composition of corrosion products and verify the identification results by FORS. Two samples of corrosion products (about 0.1 grams for each) were examined by XRD, Bruker axs (Germany) D8 Advance model, equipped with a CuKα radiation with LYNXEYE XE T detector. The XRD data were acquired in the 2θ range 4-70°in 0.02° steps and counting for 0.15s per step with scan speed of 2°/min. The voltage and current are 40 kV and 40 mA respectively. The qualitative assignment of the samples was based on the database of the Joint Committee Powder Diffraction Standards-International Center for Diffraction Data (JCPSD-ICDD) using the Jade software (version 6.5). Quantitative XRD analysis was carried out using matrix-flushing theory [54]. The percentage composition of a mixture of corrosion products was acquired.

4. Results

4.1. FORS

FORS spectra in the region from 350 to 2400nm were first acquired from 9 reference samples, in order to get reference spectra of copper-containing corrosion products commonly found on bronzes. The result shows a quite different spectral features for each spectrum of the 9 samples, especially in the SWIR region (1000-2400nm) (Fig. 3). Malachite shows a broad absorbance band between 600 nm and 900 nm [34] and two characteristic minima at 1930 nm, 2020nm and a strong, sharp one at 2270 nm. Azurite shows a reflectance maximum at about 450 nm [34,55] and a doublet strong and sharp minima at 2280 nm, 2350 nm respectively. Copper hydroxide phosphate presents a maximum at 568 nm and doublet sharp minima at 2286 nm and 2340 nm. Basic copper sulphate is characterized by the presence of a reflectance maximum at 520 nm and six absorption bands (three broad ones in the range of 650-1000 nm and 1850-2040 nm, and three sharp ones at 1430 nm, 1475nm, 2340 nm). The spectrum of copper sulphate pentahydrate is characterized by three broad absorbance bands in the range of 1400-2200 nm. FORS spectra of cuprous oxide and cupric oxide are quite different from that of other copper salts. Cupric oxide shows a broad absorption band in the 400-640 nm region, while cuprous oxide presents a narrower absorption band between 400 nm and 850 nm, followed by another one centered at 1930 nm.

The spectral characteristics of chloride-containing compounds is particularly complex, as will be illustrated below. Cuprous chloride presents a weak reflectance minimum at 1990 nm and a strong narrow one at 2350 nm. The spectral features of atacamite are centered at approximately 1465, 1855, 1987, 2159, 2339 nm, showing two minima between 1400 nm and 1600 nm, and three strong sharp absorbance band between 1800 nm and 2400 nm. The correct assignments of bands to specific chemical structure are difficult due to the lack of the spectroscopic studies in near infrared region for bronze corrosion products. However, the band at 1465 nm could be tentatively assigned to the first overtone of the OH stretching mode, and the band at 2339 nm to the combination bands of OH stretching and bending mode based on the previous spectroscopic studies [53,56]. It is worth mentioning that clinoatacamite showed very similar reflectance spectra characteristic features compared with atacamite [53]. The analysis of reference samples preliminarily demonstrated that FORS can differentiate chloride-containing compounds from other corrosion products.

In-situ FORS measurement was then conducted on 36 spots on the object surface. The reflectance spectra obtained were compared with those of references. It was found that all spots can be classified into two groups according to the spectra features. The first group including 17 sample spots could be identified as atacamite (Fig. 4). The results match well with the reflectance spectrum of atacamite reference sample used in our study as well as that of atacamite synthesized in other laboratory [53]. Another 19 detection points showed different spectral characteristics which does not match any of the reference spectrum. A doublet band at 1918, 1950 nm and two weak bands at 1422 and 1472 nm were identified. Several weak broad bands appeared in the region 1500-1900 nm (Fig. 5). According to the results of Raman and XRD, shown in the next section, these 19 samples can be identified as chalconatronite. It is difficult to assign the bands due to little studies on chalconatronite by near infrared spectroscopy. It is indeed the first time chalconatronite is identified on cultural heritage materials by FORS.

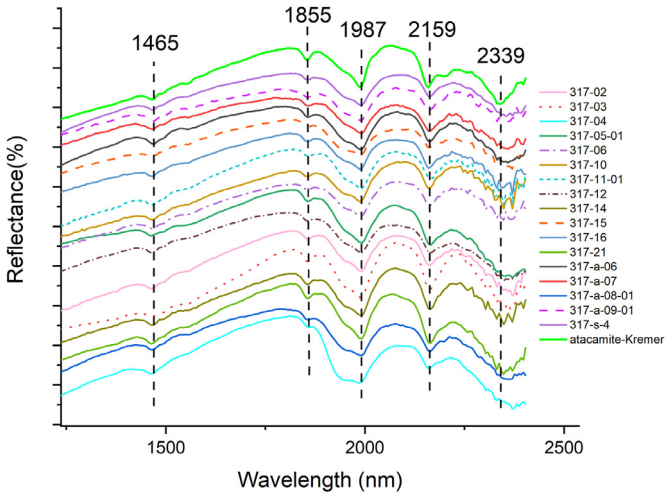

Fig. 4. Reflectance spectra of 17 samples of corrosion products on the surface of the gilded bronze statue Vajrasattva Bodhisattva. The spectrum of Kremer atacamite used as a reference is also presented for comparative analysis

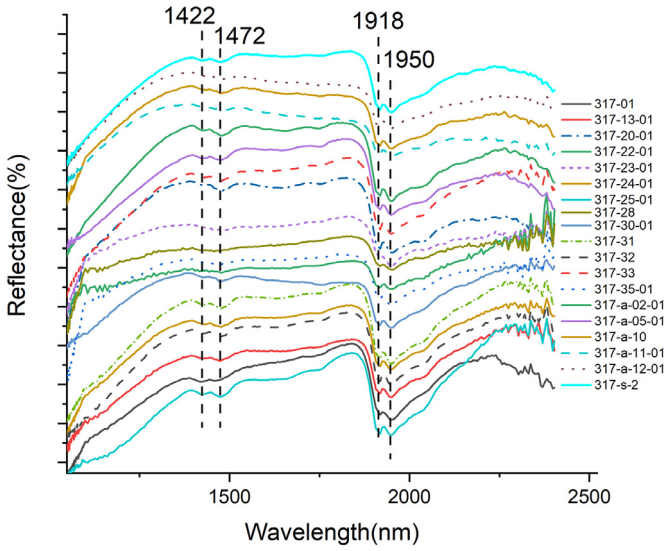

Fig. 5. Reflectance spectra of 19 samples of corrosion products on the surface of the gilded bronze statue Vajrasattva Bodhisattva. The spectra can be assigned to chalconatronite based on the XRD results of sample 317-s-2.

4.2. Raman and XRD

In order to verify the results obtained from FORS, 10 of 36 points analyzed by FORS were selected where samples were taken from the surface of the bronze statue for Raman and XRD analysis. Five of the ten samples were identified as atacamite by FORS, while for the rest five samples, the spectra did not match the reference spectra and need further confirmation.

Regarding the 5 potential atacamite samples, the Raman spectra of 3 samples (317-a-06-01, 317-a-07-03, 317-a-09-02) display bands at 118, 142, 362, 511, 820, 909, 972, 3351, 3436 cm^{-1} (Fig. 6). Another 3 spots from 2 samples (317-a-07-02, 317-a-08-02, 317-s-4) show similar characteristic peaks except a slight difference in the region 800-1000 cm^{-1} and 3000-3500 cm^{-1} (Fig. 6). They were identified as atacamite and clinoatacamite respectively by feature assignments based on the previous studies [20–23,57,58]. Both atacamite and clinoatacamite were found in sample 317-a-07. In the region 800-1000 cm^{-1}, the spectrum of atacamite has three major bands (820, 909, 972 cm^{-1}), while clinoatacamite has four bands (818, 894, 928, 971 cm^{-1}). In the region 3200-3500 cm^{-1}, the spectrum of atacamite has two major peaks at 3351, 3436 cm^{-1} and one very weak and board peak from 3310 to 3330 cm^{-1}, while clinoatacamite has three major bands at 3310, 3353, 3440 cm^{-1}. The bands, present at 909 cm^{-1} for atacamite and 894, 928, 3310 cm^{-1} for clinoatacamite, are usually used to distinguish the two copper trihydroxychlorides [57,58]. Bands at high wavenumbers between 3000 to 3500 cm^{-1} can be assigned to the OH stretching vibrations. The region between 800 to 1000 cm^{-1} can be assigned to OH deformation modes [57] or Cu-O-OH bending modes [59]. The main peak at 511 cm^{-1} for both two compounds is attributed to O-Cu-O symmetric stretching. Other bands in low wavenumber region (below 600 cm^{-1}) contain Cl-Cu-Cl bending vibration mode and O-Cu-O mode [23,57].

The rest 5 unknown samples (317-a-05-04, 317-a-10-02, 317-a-11-02, 317-a-12-01, 317-s-2) show major Raman bands at 144, 161, 328, 696, 763, 1053, 1071, 1328, 1529, 1598, 3222, 3439, 3568 cm^{-1} (Fig. 7). The identified peaks are attributable to the presence of chalconatronite ($Na_2Cu(CO_3)_2 \cdot 3H_2O$), which are in agreement with the literature [60,61]. The strong band at 327 cm^{-1} can be assigned to Cu-O stretching vibration and two very strong distinctive bands at 1053 and 1071 cm^{-1} can be attributed to carbonate symmetric stretching [61].

Two samples (317-s-2, 317-s-4) of light green corrosion products were selected for XRD analysis. The results showed sample 317-s-4 is a mixture containing 46% atacamite and 54% clinoatacamite, and sample 317-s-2 contains 100% chalconatronite. The XRD results is in good accordance with Raman, and more importantly confirm the results obtained by FORS.

Chalconatronite has been identified by XRD on many archaeological bronze objects and the reference ICDD 22-1458 was often used [4,19]. Nevertheless according to Eggert's study [62], the XRD identification of chalconatronite should be based on data derived from the crystal structures covering a larger range with truly quantitative values for intensities. The reference ICDD 01-71-1490 is recommended to use, instead of ICDD 22-1458 with limited quality. Therefore, in this study, ICDD 01-71-1490 is used for identification of chalconatronite. The charts of the X-ray diffractogram for the two samples are shown in Figs. 8 and 9. The Debye-Scherrer powder diffraction data is given in the supplementary material.

5. Discussion

5.1. The distribution "map" of bronze disease induced corrosion products

A distribution “map” containing 36 points of corrosion products on the outer and inner surface of the bronze statue was drawn, based on the results obtained by FORS. The “map” clearly showed the accurate position of two types of corrosion products including copper trihydroxychloride (atacamite and clinoatacamite) and chalconatronite. The numbers arrowed to different locations on the bronze statue refer to all samples analyzed in the study. It is easily found from the “map” that all the copper trihydroxychlorides (17 spots) analyzed are located in the frontal side, in particular on the crown, forehead, eyes, forefinger and little finger of the left hand, back and wrist of the right hand and the beading pattern on the lotus base. Most of the chalconatronite is located on left hand side, with small amount found on the back and interior of the statue (Fig. 10). This regionalized distribution pattern of two corrosion products might indicate a variation in micro-environment during the burial and storage stage, and will also greatly affect the conservation treatment strategy.

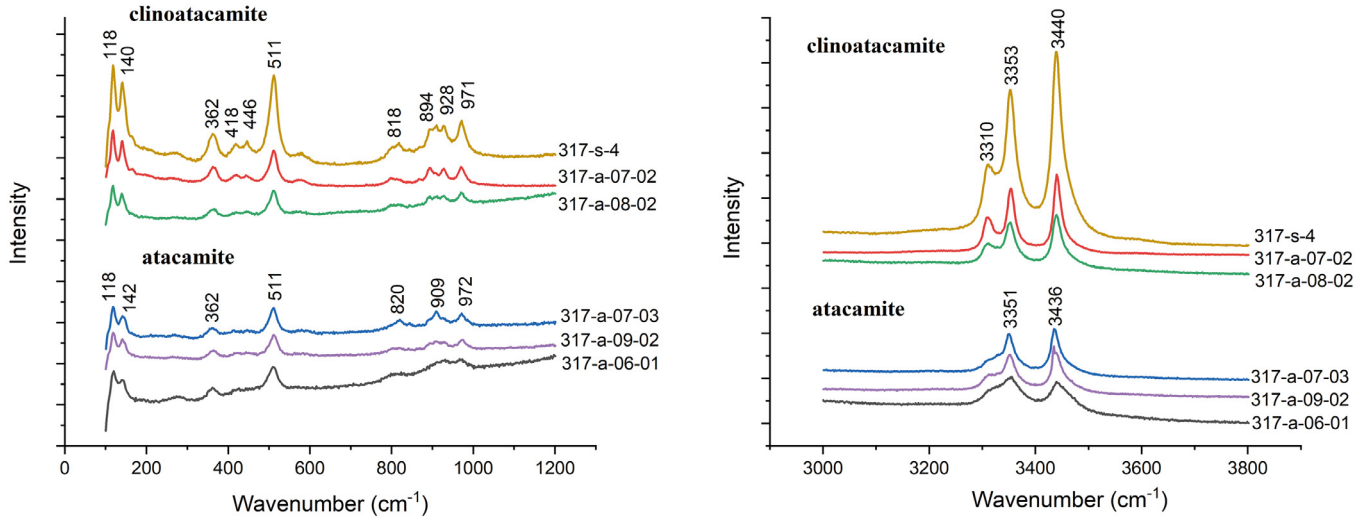

Fig. 6. Raman spectra for 6 spots from 5 corrosion products samples from the gilded bronze statue, identified as atacamite and clinoatacamite. Left: spectra at wavenumbers between 100 to1200 cm^{-1}; Right: spectra at wavenumbers between 3000 to 3800 cm^{-1}

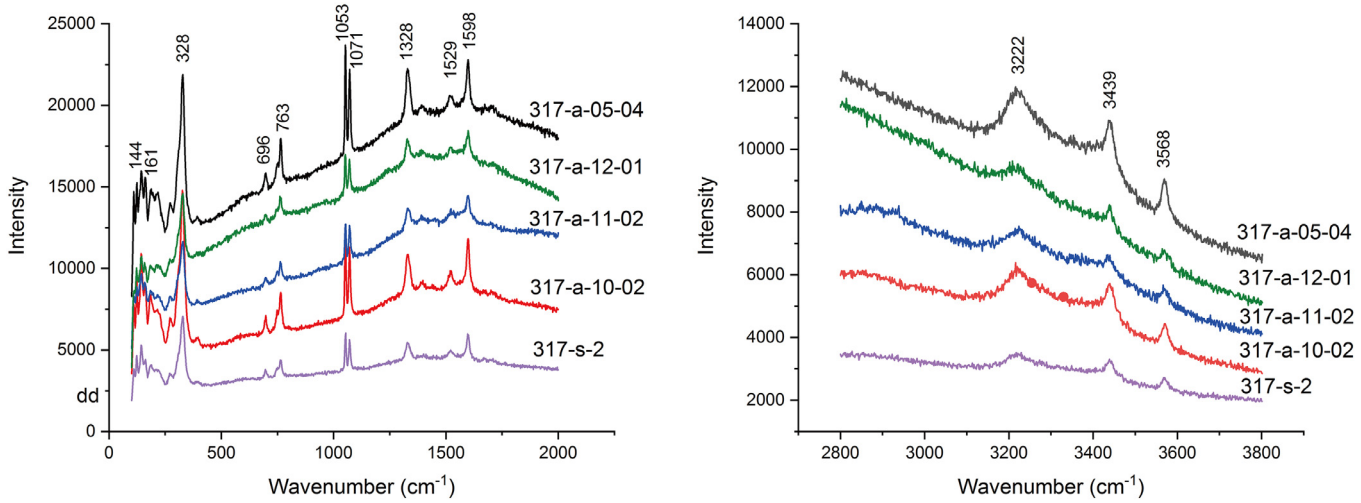

Fig. 7. Raman spectra for five corrosion products samples from the gilded bronze statue, identified as chalconatronite. Left: spectra at wavenumbers between 100 to 2000 cm^{-1}; Right: spectra at wavenumbers between 2800 to 3800 cm^{-1}

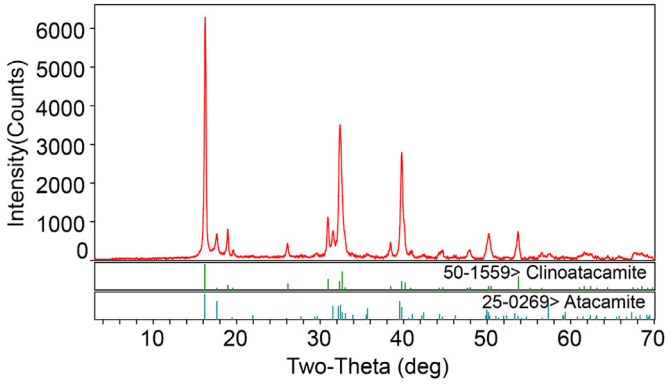

Fig. 8. The XRD diagram of the light green corrosion products identified as atacamite and clinoatacamite (sample 317-s-4)

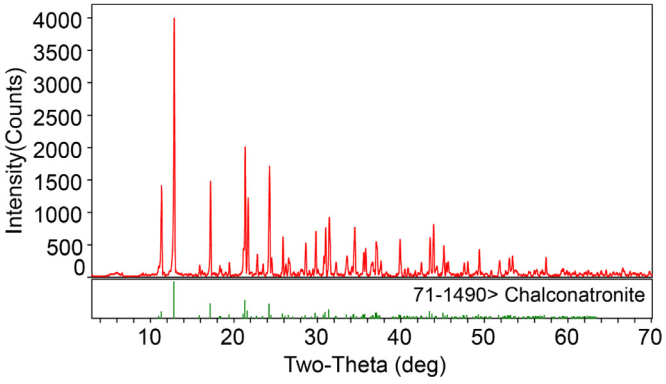

Fig. 9. The XRD diagram of the light green corrosion products identified as chalconatronite (sample 317-s-2)

5.2. The precise detection of bronze disease with FORS

Bronze disease is considered as the worst type of deterioration and most severe threat to artefact preservation. The term was first coined in 1893 and has been widely studied later by many scholars [1,3,15–18,5,6,9–14]. Generally, bronze disease is a destructive type of corrosion defined as the process of copper interacting with chloride-containing species, moisture and oxygen, resulting in the

Fig. 10. The distribution "map" of the corrosion products on the gilded bronze statue "Vajrasattva Bodhisattva". The red spots show the location of the copper trihydroxychloride and the blue spots present the location of chalconatronite.

corrosion of underlying alloy. The corrosion mechanism of bronze disease has been under investigation since its first discovery. It is now widely accepted that a self-perpetuating reaction occurs in the developing process of bronze disease. The products of the reaction are powdery and voluminous which may disrupt the original surface and disfigure the object. Objects suffering bronze disease might be perforated, or totally mineralized, and turned into a pile of powder. The general method of treating artefacts with bronze disease is to remove all chloride-bearing corrosion products and stabilize the artefacts with corrosion inhibitor.

The biggest challenge for a bronze conservator was, however, to decide whether bronze disease exist on objects and where it is located. The light green colour and powdery texture of corrosion products were previously taken as the most important indicators of bronze disease in pre-sampling stage. However, the colour and texture are affected by multiple factors including types of corrosion products, particle size and uniformity. For example, a mixture of malachite and tin oxide looks very much like the copper trihydroxychloride, and often sampled mistakenly as bronze disease induced corrosion products. This may lead to an unrepresentativeness of samples and incomplete assessment of conservation condition of objects.

The gilded bronze statue investigated in this work is covered by a large area of chalky light green corrosion products, showing typical characteristics of the copper trihydroxychloride. In regular treatment procedure, all corrosion of this type is to be removed since it might potentially trigger the self-perpetuating reaction when in contact with oxygen and moisture. Nevertheless, a complete removal of light green corrosion products would greatly alter the appearance of this artefacts and cause unreversible damage to its original morphology in certain parts. A more cautious conservation work might involve sampling several areas with light green corrosion and test them with Raman and XRD. However, as it has been demonstrated by the current study, this methodology does not guarantee a thorough assessment about the corrosion condition of artefacts.

The chance of hitting a real copper trihydroxychloride corrosion is only 50% in this case. There is little hope that the experience of conservator would help since the reflectance spectra of copper trihydroxychloride and chalconatronite present similar features in visible region (400-600 nm) (Fig. 11), rendering the discrimination by eye-balling examination not trustful. If a biased assessment had been achieved, it would cause either overtreatment by removing both unstable copper trihydroxychloride and stable chalconatronite or undertreatment by leaving chlorine-bearing minerals and threatening the longevity of the artefact.

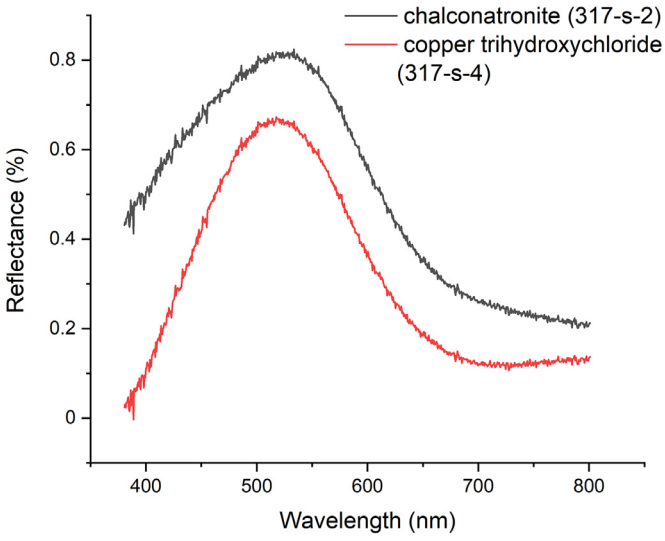

Fig. 11. The reflectance spectra of the copper trihydroxychloride and chalconatronite in the range of 380 to 800 nm.

A comprehensive FORS scan offer a new solution to this old problem. It takes less than 2 seconds to finish one analysis and a general scan for all corrosion area of an artefact of this size can be finished in less than 30 min. Its result, as it has been showcased in this study, is enough differentiative and can correctly distinguish the copper trihydroxychloride from other green corrosion products such as malachite and chalconatronite. Furthermore, FORS does not have any limitation for the size and shape of the objects, due to its working mode based on fiber. This facilitates detecting areas not easily accessible, such as the interior surface and corners. It is therefore possible to create a distribution "map" of copper trihydroxychloride with relatively high spatial resolution. On the basis of this information, a more condition-based precise treatment proposal can be generated. In this case, a regionalized

corrosion removal on the trihydroxychloride-dominated right hand side is recommended. After the treatment, another round of FORS scan would be conducted to confirm the complete clearance of Cl-bearing minerals.

Additionally, as FORS instrument is portable, it could be used for periodically measuring the artefact and monitoring the chemical change of corrosion products in museum environment, without even removing the artefacts from exhibition. In combination with general environmental data (e.g. Temperature, Relative humidity, VOC), it can greatly enhance our understanding about the mechanism of environment-induced corrosion growth on bronze artefacts and provide a key new facet on the preventive conservation.

6. Conclusions

In this study, FORS was employed to analyze the corrosion products on a gilded bronze statue "Vajrasattva Bodhisattva" dated to the Ming dynasty (A. D. 1368-1644) collected in National Museum of China. Raman and XRD were applied to confirm the results obtained by FORS. The results indicated the effectiveness of FORS for the characterization of bronze corrosion products, especially the copper trihydrochloride. It is the first time for the identification of chalconatronite by FORS. The distribution "map" of the corrosion products showing the precise position of the copper trihydroxychloride and chalconatronite, was drawn based on the FORS results, allowing for the first time to get a relatively comprehensive assessment of corrosion products on this artefact.

This is a pilot study to explore the possibility of FORS for the identification of complex and highly varied bronze corrosion products. The application of FORS on corrosion products would change the traditional way of condition assessment of bronze objects, and help conservators make condition-based precise conservation proposals.

Admittedly, there are some limitations in using FORS to identify the corrosion products, in terms of spatial resolution and identification of minerals from mixtures. In order to resolve these issues, we are establishing a database comprising various types of bronze corrosion products formed in different burial and storing conditions. On the basis of extensive corrosion products database, a machine learning algorithm could be developed to differentiate corrosion products from complex mixtures, in particular identifying chloride-containing corrosion products. Facilitated by this algorithm, the hyperspectral imaging would be used to map the distribution of different bronze corrosion products on the surface.

Acknowledgments

This research is supported by National Key Research and Development Project of China (2019YFC1520205, 2020YFC1521606) and Giant Subject of National Social Science Foundation of China (17ZDA219) and National Cultural Heritage Administration Key Scientific Research Base Project (2020ZCK111). Acknowledgments are attributed to Professor Haida Liang, director of Imaging, Materials and Engineering Center (IMEC) in Nottingham Trent University for the contribution of the initial idea about this study and the useful discussions and suggestions. Thanks should also go to Liang Qu and Guanghua Li from the Palace Museum in China for providing Kremer pigments.

Supplementary materials

Supplementary material associated with this article can be found, in the online version, at doi:10.1016/j.culher.2021.03.007.

References

[1] I. Macleod, Bronze Disease : An Electrochemical Explanation, ICCM Bull. VII (1981) 16–26, doi:10.1179/iccm.1981.7.1.002.
[2] W.T. Chase, Chinese Bronzes: Casting, Finishing, Patination, and Corrosion, Technol. Mediev. Jewel. (1992) 85–182.
[3] D.A. Scott, Bronze Disease : A Review of Some Chemical Problems and the Role of Relative Humidity, J. Am. Inst. Conserv. 29 (1990) 193–206.
[4] D.A. Scott, L. Swartz Dodd, Examination, conservation and analysis of a gilded Egyptian bronze Osiris, J. Cult. Herit. 3 (2002) 333–345, doi:10.1016/S1296-2074(02)01238-4.
[5] D.A. Scott, Copper and Bronze in Art: corrosion, colorants, conservation, Getty Publications, Los Angeles, Califarnia, United States, 2002.
[6] L. Robbiola, J.M. Blengino, C. Fiaud, Morphology and mechanisms of formation of natural patinas on archaeological Cu-Sn alloys, Corros. Sci. 40 (1998) 2083–2111, doi:10.1016/S0010-938X(98)00096-1.
[7] M.P. Casaletto, G.M. Ingo, M. Albini, A. Lapenna, I. Pierigè, C. Riccucci, F. Faraldi, An integrated analytical characterization of corrosion products on ornamental objects from the necropolis of Colle Badetta-Tortoreto (Teramo, Italy), Appl. Phys. A Mater. Sci. Process. 100 (2010) 801–808, doi:10.1007/s00339-010-5675-3.
[8] M. Taube, A.H. King, W.T. Chase, Transformation of ancient Chinese and model two-phase bronze surfaces to smooth adherent patinas, Phase Transitions 81 (2008) 217–232, doi:10.1080/01411590701514375.
[9] S. Aouadi, N. Souissi, Early stages of tin bronze corrosion in neutral aqueous chloride media: Electrochemical and FTIR investigations, Mater. Corros. 67 (2016) 1105–1113, doi:10.1002/maco.201608856.
[10] V.F. Lucey, Mechanism of pitting corrosion of copper in supply water, Br. Corros. J. 2 (1967) 175–185.
[11] D.A. Scott, Metallography and Microstructure of Ancient and Historic Metals, The Getty Conservation Institue and Archetype Books, Singapore, 1991.
[12] D.A. Scott, A Review of Copper Chlorides and Related Salts in Bronze Corrosion and as Painting Pigments, Stud. Conserv. 45 (2000) 39–53.
[13] D.A. Scott, New insights on the corrosion of ancient bronzes using X-ray powder diffraction: The importance of paratacamite, sampleite, and connellite, Stud. Conserv. 62 (2017) 410–418, doi:10.1080/00393630.2016.1219466.
[14] G.M. Ingo, T. De Caro, C. Riccucci, E. Angelini, S. Grassini, S. Balbi, P. Bernardini, D. Salvi, L. Bousselmi, A. Çilingiroğlu, M. Gener, V.K. Gouda, O.A.L. Jarrah, S. Khosroff, Z. Mahdjoub, Z.A.L. Saad, W. El-Saddik, P. Vassiliou, Large scale investigation of chemical composition, structure and corrosion mechanism of bronze archeological artefacts from Mediterranean basin, Appl. Phys. A Mater. Sci. Process. 83 (2006) 513–520, doi:10.1007/s00339-006-3550-z.
[15] A. Mezzi, E. Angelini, T. De Caro, S. Grassini, F. Faraldi, C. Riccucci, G.M. Ingo, Investigation of the benzotriazole inhibition mechanism of bronze disease, Surf. Interface Anal. 44 (2012) 968–971, doi:10.1002/sia.4841.
[16] B. Bozzini, B. Alemán, M. Amati, M. Boniardi, V. Caramia, G. Giovannelli, L. Gregoratti, M.Kazemian Abyaneh, Novel insight into bronze disease gained by synchrotron-based photoelectron spectro-microscopy, in support of electrochemical treatment strategies, Stud. Conserv. 62 (2017) 465–473, doi:10.1080/00393630.2016.1235339.
[17] C.G. Fink, Periodic formation of corrosion products, in: H.H. Uhlig (Ed.), Corros. Handb., J. Wiley, New York, 1948, pp. 103–105.
[18] R.M. Organ, Aspects of bronze patina and its treatment, Stud. Conserv. 8 (1963) 1–9, doi:10.1179/sic.1963.002.
[19] Q. Wang, H. Huang, F. Shearman, Bronzes from the Sacred Animal Necropolis at Saqqara, Egypt: a study of the metals and corrosion, Br. Museum Tech. Res. Bull. 3 (2009) 73–82.
[20] W. Martens, R.L. Frost, P.A. Williams, Raman and infrared spectroscopic study of the basic copper chloride minerals - Implications for the study of the copper and brass corrosion and "bronze disease, Neues Jahrb. Fur Mineral. Abhandlungen. 178 (2002) 197–215, doi:10.1127/0077-7757/2003/0178-0197.
[21] W. Martens, R.L. Frost, J.T. Kloprogge, P.A. Williams, Raman spectroscopic study of the basic copper sulphates - Implications for copper corrosion and "bronze disease, J. Raman Spectrosc. 34 (2003) 145–151, doi:10.1002/jrs.969.
[22] R.L. Frost, W. Martens, J.Theo Kloprogge, P.A. Williams, Raman spectroscopy of the basic copper chloride minerals atacamite and paratacamite: Implications for the study of copper, brass and bronze objects of archaeological significance, J. Raman Spectrosc. 33 (2002) 801–806, doi:10.1002/jrs.921.
[23] A. Coccato, D. Bersani, A. Coudray, J. Sanyova, L. Moens, P. Vandenabeele, Raman spectroscopy of green minerals and reaction products with an application in Cultural Heritage research, J. Raman Spectrosc. 47 (2016) 1429–1443, doi:10.1002/jrs.4956.
[24] A. Casini, M. Bacci, C. Cucci, F. Lotti, S. Porcinai, M. Picollo, B. Radicati, M. Poggesi, L. Stefani, Fiber optic reflectance spectroscopy and hyper-spectral image spectroscopy: two integrated techniques for the study of the Madonna dei Fusi, Opt. Methods Arts Archaeol. 5857 (2005) 58570M, doi:10.1117/12.611500.
[25] M. Bacci, M. Picollo, G. Trumpy, M. Tsukada, D. Kunzelman, Non-Invasive Identification of White Pigments on 20th-Century Oil Paintings by Using Fiber Optic Reflectance Spectroscopy, J. Am. Inst. Conserv. 46 (2007) 27–37.
[26] I. Garofano, J.L. Perez-Rodriguez, M.D. Robador, A. Duran, An innovative combination of non-invasive UV–Visible-FORS, XRD and XRF techniques to study Roman wall paintings from Seville, Spain, J. Cult. Herit. 22 (2016) 1028–1039, doi:10.1016/j.culher.2016.07.002.
[27] L. Pronti, A.C. Felici, M. Ménager, C. Vieillescazes, M. Piacentini, Spectral Behavior of White Pigment Mixtures Using Reflectance, Ultraviolet—Fluorescence Spectroscopy, and Multispectral Imaging, Appl. Spectrosc. 71 (2017) 2616–2625, doi:10.1177/0003702817717969.

[28] S. Gasanova, S. Pagès-Camagna, M. Andrioti, S. Hermon, Non-destructive in situ analysis of polychromy on ancient Cypriot sculptures, Archaeol. Anthropol. Sci. 10 (2018) 83–95, doi:10.1007/s12520-016-0340-1.
[29] C. Miliani, F. Rosi, A. Daveri, B.G. Brunetti, Reflection infrared spectroscopy for the non-invasive in situ study of artists' pigments, Appl. Phys. A. 106 (2012) 295–307.
[30] E. Cheilakou, M. Kartsonaki, M. Koui, P. Callet, A nondestructive study of the identification of pigments on monuments by colorimetry, Int. J. Microstruct. Mater. Prop. 4 (2009) 112–127, doi:10.1504/IJMMP.2009.028437.
[31] E. Cheilakou, M. Troullinos, M. Koui, Identification of pigments on Byzantine wall paintings from Crete (14th century AD) using non-invasive Fiber Optics Diffuse Reflectance Spectroscopy (FORS), J. Archaeol. Sci. 41 (2014) 541–555, doi:10.1016/j.jas.2013.09.020.
[32] F. Rosi, C. Miliani, C. Clementi, K. Kahrim, F. Presciutti, M. Vagnini, V. Manuali, A. Daveri, L. Cartechini, B.G. Brunetti, A. Sgamellotti, An integrated spectroscopic approach for the non-invasive study of modern art materials and techniques, Appl. Phys. A. 100 (2010) 613–624.
[33] P. Ricciardi, J.K. Delaney, M. Facini, L. Glinsman, Use of imaging spectroscopy and in situ analytical methods for the characterization of the materials and techniques of 15th century illuminated manuscripts, J. Am. Inst. Conserv. 52 (2013) 13–29, doi:10.1179/0197136012Z.0000000004.
[34] A. Cosentino, FORS Spectral Database of Historical Pigments in Different Binders, E-Conservation J (2014) 54–65, doi:10.18236/econs2.201410.
[35] S. Kogou, A. Lucian, S. Bellesia, L. Burgio, K. Bailey, C. Brooks, H. Liang, A holistic multimodal approach to the non-invasive analysis of watercolour paintings, Appl. Phys. A Mater. Sci. Process. 121 (2015) 999–1014, doi:10.1007/s00339-015-9425-4.
[36] S. Kogou, S. Neate, C. Coveney, A. Miles, D. Boocock, L. Burgio, C.S. Cheung, H. Liang, The origins of the Selden map of China: Scientific analysis of the painting materials and techniques using a holistic approach, Herit. Sci. 4 (2016) 1–24, doi:10.1186/s40494-016-0098-x.
[37] M. Aceto, A. Agostino, G. Fenoglio, A. Idone, M. Gulmini, M. Picollo, P. Ricciardi, J.K. Delaney, Characterisation of colourants on illuminated manuscripts by portable fibre optic UV-visible-NIR reflectance spectrophotometry, Anal. Methods. 6 (2014) 1488–1500, doi:10.1039/c3ay41904e.
[38] M.A. Maynez-Rojas, E. Casanova-González, J.L. Ruvalcaba-Sil, Identification of natural red and purple dyes on textiles by Fiber-optics Reflectance Spectroscopy, Spectrochim. Acta - Part A Mol. Biomol. Spectrosc. 178 (2017) 239–250, doi:10.1016/j.saa.2017.02.019.
[39] R. Nakamura, M. Naruse, Spectroscopic Analysis of Colorants Used for bachiru Carving Technique Found in the Shosoin Treasures, Stud. Conserv. 63 (2018) 267–276, doi:10.1080/00393630.2017.1341010.
[40] E. Calà, F. Gosetti, M. Gulmini, I. Serafini, A. Ciccola, R. Curini, A. Salis, G. Damonte, K. Kininger, T. Just, M. Aceto, It's only a part of the story: Analytical investigation of the inks and dyes used in the privilegium maius, Molecules 24 (2019), doi:10.3390/molecules24122197.
[41] M. Vagnini, C. Miliani, L. Cartechini, P. Rocchi, FT-NIR spectroscopy for non-invasive identification of natural polymers and resins in easel paintings, Anal. Bioanal. Chem. 395 (2009) 2107–2118, doi:10.1007/s00216-009-3145-6.
[42] A. Pallipurath, R.V. Vofély, J. Skelton, P. Ricciardi, S. Bucklow, S. Elliott, Estimating the concentrations of pigments and binders in lead-based paints using FT-Raman spectroscopy and principal component analysis, J. Raman Spectrosc. 45 (2014) 1272–1278, doi:10.1002/jrs.4525.
[43] M. Reháková, L. Gál, M. Belovičová, M. Oravec, V. Dvonka, D. Stojkovičová, M. Čeppan, Identification of iron-gall inks in historical drawings by Fibre Optics Reflection Spectroscopy – Extension to the NIR spectral range, J. Cult. Herit. 27 (2017) 137–142, doi:10.1016/j.culher.2017.03.005.
[44] A. Methods, C. Amctb, UV-visible-NIR reflectance spectrophotometry in cultural heritage: Background paper, Anal. Methods. 8 (2016) 5894–5896, doi:10.1039/c6ay90112c.
[45] N. Odisio, M. Calabrese, A. Idone, N. Seris, L. Appolonia, J.M. Christille, Portable Vis-NIR-FORS instrumentation for restoration products detection: Statistical techniques and clustering, Eur. Phys. J. Plus. 134 (2019) 1–16, doi:10.1140/epjp/i2019-12469-5.
[46] S. Zaleski, E. Montagnino, L. Brostoff, I. Muller, A. Buechele, C.Lynn Ward-Bamford, F. France, M. Loew, Application of fiber optic reflectance spectroscopy for the detection of historical glass deterioration, J. Am. Ceram. Soc. 103 (2020) 158–166, doi:10.1111/jace.16703.
[47] C. Cucci, L. Bigazzi, M. Picollo, Fibre Optic Reflectance Spectroscopy as a non-invasive tool for investigating plastics degradation in contemporary art collections: A methodological study on an expanded polystyrene artwork, J. Cult. Herit. 14 (2013) 290–296, doi:10.1016/j.culher.2012.08.003.
[48] D. Han, L. Ma, S. Ma, J. Zhang, The digital restoration of painted patterns on the No. 2 Qin bronze chariot based on hyperspectral imaging, Archaeometry 62 (2020) 200–212, doi:10.1111/arcm.12516.
[49] F. Grazzi, C. Cucci, A. Casini, L. Stefani, N. Kardjilov, A. Thiele, J. Hosek, M. Picollo, Merging of imaging techniques based on reflectance hyperspectral and neutron tomography for characterization of a modern replica of a 13th century knife from Croatia, Proc. SPIE. 11058 (2019) 1–13, doi:10.1117/12.2526050.
[50] B. Grabowski, W. Masarczyk, P. Głomb, A. Mendys, Automatic pigment identification from hyperspectral data, J. Cult. Herit. 31 (2018) 1–12, doi:10.1016/j.culher.2018.01.003.
[51] L. Yong, Copper trihydroxychlorides as pigments in China, Stud. Conserv. 57 (2012) 106–111, doi:10.1179/2047058411Y.0000000008.
[52] G.H. Li, Y. Chen, X.J. Sun, P.Q. Duan, Y. Lei, L.F. Zhang, An automatic hyperspectral scanning system for the technical investigations of Chinese scroll paintings, Microchem. J. 155 (2020), doi:10.1016/j.microc.2020.104699.
[53] E. Catelli, G. Sciutto, S. Prati, Y. Jia, R. Mazzeo, Characterization of outdoor bronze monument patinas: the potentialities of near-infrared spectroscopic analysis, Environ. Sci. Pollut. Res. 25 (2018) 24379–24393, doi:10.1007/s11356-018-2483-3.
[54] F.H. Chung, Quantitative interpretation of X-ray diffraction patterns of mixtures. I. Matrix-flushing method for quantitative multicomponent analysis, J. Appl. Crystallogr. 7 (1974) 526–531.
[55] R.L.M. Bacci, R.Carlà F.Baldini, A color analysis of the Brancacci Chapel Frescoes, Appl. Spectrosc. 45 (1991) 26–31, doi:10.1366/0003702914337713.
[56] R.L. Frost, B.J. Reddy, D.L. Wain, W.N. Martens, Identification ofthe rosasite group minerals—an application ofnear infrared spectroscopy, Spectrochim Acta Part A 66 (2007) 1075–1081.
[57] G. Bertolotti, D. Bersani, P.P. Lottici, M. Alesiani, T. Malcherek, J. Schlüter, Micro-Raman study of copper hydroxychlorides and other corrosion products of bronze samples mimicking archaeological coins, Anal. Bioanal. Chem. 402 (2012) 1451–1457, doi:10.1007/s00216-011-5268-9.
[58] M. Bouchard, D.C. Smith, Catalogue of 45 reference Raman spectra of minerals concerning research in art history or archaeology, especially on corroded metals and coloured glass, Spectrochim. Acta Part A. 59 (2003) 2247–2266, doi:10.1016/S1386-1425(03)00069-6.
[59] X. Liu, D. Meng, X. Zheng, M. Hagihala, Q. Guo, Mid-IR and Raman spectral properties of clinoatacamite-structure basic copper chlorides, Adv. Mater. Res. 146–147 (2011) 1202–1205, doi:10.4028/www.scientific.net/AMR.146-147.1202.
[60] C. Chiavari, C. Martini, S. Montalbani, E. Franzoni, M.C. Bignozzi, M.C. Passeri, The bronze panel (paliotto) of San Moisè in Venice: materials and causes of deterioration, Mater. Corros. 67 (2016) 141–151.
[61] A. Fischer, G. Eggert, J. Stelzner, When Glass and Metal Corrode Together, VI: Chalconatronite, Stud. Conserv. 65 (2020) 152–159, doi:10.1080/00393630.2019.1677081.
[62] G. Eggert, A. Fischer, R.E. Dinnebier, One heritage corrosion product less: Basic sodium copper carbonate, Herit. Sci. 4 (2016) 3–7, doi:10.1186/s40494-016-0092-3.